Acta Astronautica 240 (2026) 63–75

Contents lists available at ScienceDirect

Acta Astronautica

journal homepage: www.elsevier.com/locate/actaastro

LunarLeaper—A mission concept to explore the lunar subsurface with a small-scale legged robot☆

Hendrik Kolvenbach [a,*], Anna Mittelholz [b], Simon C. Stähler [c], Philip Arm [a], Valentin T. Bickel [d], Adrian Fuhrer [a], Jordi Gomez Jodar [b], Ramon Margarit [b], Joseph Church [a], Elena Krasnova [a], Krzysztof Walas [e], Matthias Grott [f], Svein-Erik Hamran [g], Özgür Karatekin [h], Miguel Olivares-Mendez [i], Sofia Coloma [i], Marco Pagnamenta [j], Michał Gumiela [k], Jordan Aaron [b], Marco Hutter [a]

[a] Robotic Systems Lab, ETH Zurich, Switzerland
[b] Earth and Planetary Sciences, ETH Zurich, Switzerland
[c] Space Systems and Technology, ETH Zurich, Switzerland
[d] Center for Space and Habitability, University of Bern, Switzerland
[e] Institute of Robotics and Machine Intelligence, Poznan University of Technology, Poland
[f] Institute of Planetary Research, German Aerospace Center, Germany
[g] Department of Technology Systems, University of Oslo, Norway
[h] Royal Observatory of Belgium, Belgium
[i] Space Robotics Research Group, University of Luxembourg, Luxembourg
[j] RIVR Technologies AG, Switzerland
[k] KP Labs sp. z o.o., Poland

ARTICLE INFO

Keywords:
LunarLeaper
Legged robot
Lunar lava tubes
Marius hills pit
Lunar exploration
Autonomous planetary robotics
Ground penetrating radar
Lunar subsurface
Geophysical survey
Lunar mission concept

ABSTRACT

We present the LunarLeaper mission concept, which aims to robotically investigate volcanic pits on the lunar surface. Volcanic pits, or skylights, are collapse features that may provide access to subsurface lava tubes, which could serve as shelters for future human explorers and offer insight into the volcanic history of the Moon by exposing ancient lava flows. The existence and extent of large caves are still debated today and require in situ analysis. The Marius Hills site in particular offers a potential entry point to a cave system in a volcanic region on the lunar nearside. Our mission aims to deploy a payload-equipped 15 kg-class legged robot that can approach a pit, such as the Marius Hills pit, while taking measurements during the traverse. During the mission, measurements from a ground-penetrating radar (GPR) and a gravimeter will allow us to survey the subsurface and map any underlying lava tube, if present. The mission will investigate key questions regarding lunar volcanism, such as the existence and geometry of subsurface caves and the magnitude and timing of lava flows, while assessing the site's suitability for future human utilization and habitation. Furthermore, the mission will demonstrate key enabling technologies such as legged robots, serving as building blocks for the next generation of planetary missions.

1. Introduction

To this day, close to 300 pits have been identified on the lunar surface by the means of remote sensing [1]. Pits are collapse features usually located in impact melt and mare regions, and are of high scientific interest because they expose the local (volcanic) stratigraphic record and provide access to subterranean, ancient, and possibly large lava tubes. Those lava tubes could serve as natural shelters for future astronauts, protecting them from harsh surface conditions such as radiation, extreme temperatures, and impact bombardment [1,2]. Lunar pits expose the sequence of volcanic flows along their walls, offering a unique opportunity to study the Moon's subsurface and thus geologic history in detail; the exposed stratigraphic record provides insights into the evolution of the lunar surface and the timing of volcanic activity, as well as changes of composition over time.

☆ This article is part of a Special issue entitled: '2024 75th IAC Milan' published in Acta Astronautica.

* Corresponding author.
E-mail address: hendrikk@ethz.ch (H. Kolvenbach).

https://doi.org/10.1016/j.actaastro.2025.11.039
Received 27 February 2025; Received in revised form 15 May 2025; Accepted 14 November 2025
Available online 21 November 2025

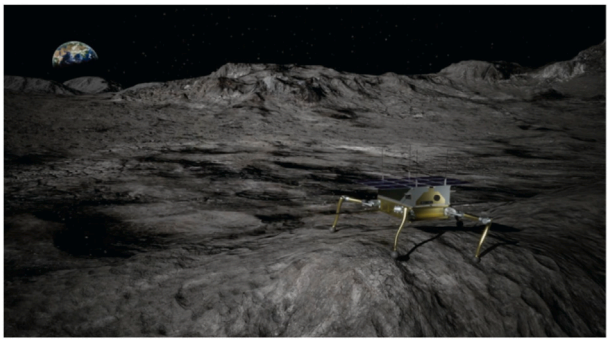

Fig. 1. Artist impression of the LunarLeaper robot approaching a skylight.

In this context, the Marius Hills Pit (MHP) is particularly interesting because it is located in Oceanus Procellarum, a mare area shaped by extensive volcanic activity in the past. Moreover, a clear topographic expression (Fig. 3) suggests the presence of an underlying lava tube, making MHP a promising site for subsurface investigation. With a diameter of approximately 50 m, the distances required to investigate the pit and surrounding area are feasible for robotic exploration [3,4]. Orbital imaging and geophysical observations suggest the MHP features pronounced layering in its wall and could be an entryway to a lava tube [5–7]. Although we will focus on exploration of the MHP for the remainder of this paper, we note that several other pits represent potential target sites. For example, a recent publication [8] provides further indication for a cave conduit at the Mare Tranquillitatis pit.

Current analyses of lunar pits are constrained by the limited spatial resolution and imaging geometry of orbital assets, preventing the identification of anything beyond a potentially small void space beneath the pit. Only a surface mission can provide the next step in confirming and characterizing potential subsurface cave systems — which in turn could provide ground truth data to increase the confidence in potential orbital cave detections in other locations.

The MHP has previously been considered by other mission concepts [3,4], often involving large, costly rovers or cranes designed to access a potential lava tube beneath the pit. However, implementing such concepts presents major challenges due to the rugged, uneven, and sloped terrain, particularly at increasingly steep slopes in the funnel region that represent the transition between the surrounding terrain and the approximately vertical pit wall [1] (Fig. 4). A further challenge arises from the unknown physical stability of the terrain along the pit funnel, let alone the uncertainty regarding the existence of a larger cave.

While wheeled rovers offer advantages in simplicity, cost, and component heritage, they are fundamentally limited in accessing such environments. Especially in view of steep, uneven, and possibly loose terrain at the MHP, the ability of wheeled rovers to traverse would be severely restricted, reducing the capability to image into the pit and achieving key mission objectives. Furthermore, legs offer the advantage of being able to manipulate the environment, where otherwise mechanical arms would be required, increasing mechanical complexity and mass.

A legged robot inherently offers superior mobility on rugged and irregular surfaces [9–11]. Examples include ETHs SpaceBok [12] and ANYmal [13], which both demonstrated mobility on 25 degrees inclined planetary analog soil [14,15]. Their ability to carefully place feet, dynamically adapt posture, and negotiate slopes and obstacles allows them to maintain proximity to the funnel of the pit and conduct close-up investigations. The flexible platform can also adapt to specific positions required by instruments, eliminating the need for camera articulation or other instrumentation. This agility is crucial to maximize scientific return, particularly in a region where precise maneuvering is essential to ensure the safety of the system. Thus, we propose a novel, 15-kg-class legged robot to perform the mission and demonstrate legged locomotion as a key technology for future lunar exploration missions (see Fig. 1).

In the following, we will present the science and technology goals in Section 2, the mission concept in Section 3, the payload suite and robotic system in Sections 4 and 5, respectively, before discussing mission implementation in Section 6, the conclusion in Section 7, and the outlook in Section 8.

2. Science and technology goals

In order to maximize the scientific return of the mission, we have defined a set of key scientific and technology objectives that will guide our exploration strategy, robot design, and instrument deployment.

2.1. Scientific objectives

We expect to address a number of detailed scientific mission objectives (O1–O4), which are also displayed in the Science Traceability Matrix in Fig. 2:

O1 - Investigate subsurface lava tubes: The primary objective of the mission is to investigate the existence and extent of subsurface caves. By combining high-resolution local ground surveys with available orbital observations, we can gain further insight into regional geology, thus going beyond a local study of the selected landing site/pit.

O2 - Assess the suitability of lava tubes for human exploration and habitation: First, it is suspected that the lava tubes could span hundreds of kilometers, yet only ~300 pits have been located so far. This raises the question of why the collapse occurred and whether a further collapse is likely. Another critical aspect in the assessment of suitability for a lunar base is the structure of the floor of the cave and the accessibility and terrain around the pit. The capabilities of the legged robot allow us to approach the pit and determine the accessibility and stability of the pit funnel with large robotic (crane-) systems or other types of equipment, as well as assess its resistance to impact bombardment. Assessment of mineralogy around the pit will provide important information on the availability of potential resources.

O3 - Assess geological processes, specifically the volcanic evolution of the Moon: Surface-exposed bedrock outcrops are exceedingly rare on the lunar surface. However, exposed stratigraphy is uniquely accessible along a pit wall [6] and allows addressing questions about lava flow emplacement, including the number of flows, their volume, and timescales, central to understanding lunar volcanism and thus a key aspect of the Moon's geologic evolution in general. Layers of paleoregolith between individual lava flows might be present if a significant pause in volcanic activity occurred, allowing for space weathering and impact gardening to fracture the exposed surface rock and create regolith. Such layers are of particular interest because they reveal pauses in the Moons volcanic activity and might encode records of past solar activity [16]. Lunar mare basalts are enriched in FeO and TiO_2, depleted in Al_2O_3 and are thought to be a product of the remelting of mantle cumulates from early differentiation [17]. Thus, changes in the composition as exposed along the pit wall provide insights into the evolution of magma sources over time. The combination of pit wall observations with geophysical observations of the shallow subsurface around the pit allow us to extend the localized view at the pit to a more regional one.

O4 - Investigate the local and regional extent of regolith: The regolith is the result of weathering and the thickness of the regolith layers is thus indicative of the time it has been exposed to space; as such the thickness of regolith with possible variations along the traverse provides important information about the regional geological history. Note that recent regolith thickness measurements from the Chinese ground-penetrating radar (GPR) on their Chang'e-4 mission provide points for comparison [18–20]. A source of uncertainty are the physical, geomechanical properties of the regolith around and on the funnel of the pit. Both aspects are highly relevant for future ISRU and exploration activities [21], as discussed in the context of O2. Layers that are not exposed to space, but that are accessible from inside a subsurface cave/tube, represent unique sample sites for future missions.

(A) Science Objective and Hypotheses	(B) Science Exploration / Investigation	(C) Investigation Objective Requirements			(D) Mission Top Level Requirements
		Measurement	Requirements	Expected	
(O1) Investigate subsurface lava tubes	**Is a lava tube present?** **What is the extent of the lava tube?** Does subsurface structure follow the topographic and/or other orbital indications for a lava tube?	- Identify a reflector compatible with a void in the ground radar data - Identify the gravimetric signature of a mass deficit compatible with a subsurface void - Determine the lateral extent of the subsurface void and compare to inferred geometry, e.g. of rille interpreted as the boundary of a lava tube. - Images of the lower part and/or floor of the pit if possible.	**GPR:** Penetration depth minimum: 2 m maximum: 70 m Resolution: 5 m SNR: 10 dB rel. to noise for reflector at 70 m. **GRAV:** Measure gravitational acceleration to <20 μ Gal precision. Detect 20 m diameter lava tube at 30 m depth (~ 1 mGal) **SCAM:** Resolution <10 cm at 100 m distance for the entire pit wall. Color images. **SPEC:** Pointing accuracy 10s of mrad. Thermal IR: 7.5-10.5 μm, upscope: 3 sensor heads (5-8 μm and 10-14 μm)	**GPR:** RIMFAX2.0 We expect to be able to detect caves down to 100 meters below the surface. Antenna frequency < 100 MHz **GRAV:** Based on GRASS with <10 μGal precision. **SCAM:** FoV 40 deg, 2048x2048 pixels, resolution < 5 cm at 100 m. **SPEC:** Fabry Perot Interferometer, 7.5-10.5 μm (thermal IR)	Provision, deployment, and operation of a lander and robot with context and navigation cameras and >1 km traverse capabilities. Accommodation of payload on robot (GPR, GRAV, SCAM, SPEC). Communications link between robot and lander and between lander and Mission Operations Center on Earth. Relay of data to Lander platform and Science Team on Earth. Landing Site within 500 m of pit. Operation duration of 1 lunar day.
(O2) Assess the suitability of lava tubes for human exploration and habitation	**Why did the pit collapse?** Can we identify pre-existing discontinuities? How stable is the pit currently? **How could the pit be accessed?** What is the potential for resource utilization?	- High resolution images of the pit to identify the fracture network, with characteristic, and potentially asymmetric fracture patterns. - Geomechanical measurements of the regolith around the pit and along the pit edge (looser regolith could be sign for impact ejecta). - Density and strength properties of the basalt and regolith. - Variations in regolith depth. - Distribution of boulders around the pit (impact ejecta vs collapse residuals). - Spectral assessment of pit layers and surroundings.			
(O3) Assess geological processes, specifically volcanic evolution of the Moon	**Characterize evolution and timing of lunar volcanism as recorded along the pit wall:** How thick are individual layers along the exposed pit wall, do they vary in composition? Is the layering interrupted by paleoregolith layers indicative of pausing eruption activity? What is the flow morphology of the basaltic layers? What is the density, porosity of the basaltic layers? **Constrain regional geological history of the Marius Hills volcanic complex at the surface and shallow subsurface:** What is the layering along the traverse and is it consistent with layering along the pit wall? What is the effect of impact craters on subsurface structure and surface composition? How does the ground-truth, i.e. surface data compare with orbital measurements?	- High resolution stereo images and spectral data along the pit wall to be put in context with regional geophysical survey. - GPR and gravity measurements along the traverse to identify and characterize individual layers regionally. - Contrast geophysical measurements inside and outside impact craters. - Images and spectral measurements along the traverse with a focus on ROIs such as blocks or craters.			
(O4) Investigate the local and regional extent of regolith	**What is the regolith thickness?** What is the surface/substructure of the regolith? Are there multiple layers of regolith and if so, do they vary in composition and/or structure? **What are geomechanical properties of the regolith?** How does the layering differ from previously investigated sites?	- High resolution stereo images and, if possible, spectral data along the pit wall to be put in context with regional geophysical survey. - GPR and gravity measurements along the traverse to identify and characterize individual layers regionally. - Geomechanical measurements of the regolith around the pit.			

Fig. 2. The Science Traceability Matrix for the LunarLeaper mission.

2.2. Technical demonstration objectives

Beside the scientific objectives, we propose unique technical demonstration objectives (T1–T5). Primarily, the deployment of a legged robot will be a validation of this locomotion concept for exploration. This will create future opportunities for applications on the Moon and beyond. Furthermore, the mission will validate several technologies related to robot design, actuation, and learning-based control.

T1 - Robotic walking on the lunar surface: The objective is to demonstrate the robot's ability to walk on the lunar surface. The hypothesis is that the robot can move forward using mechanical legs, switch between walking modes to navigate various terrains, overcome certain steepness and obstacles, and maintain operational efficiency while reducing risks. Key performance indicators (KPIs) will include speed, gait transitions, terrain steepness, obstacle size, efficiency as Cost of Transport (COT), and recovery from failures. In total, we estimate a 500 m traverse to reach the main objectives, and overcoming slopes of 15–25 degrees as well as rocks up to a defined size, with stretch goals targeting greater distances, dynamic walking, steeper terrain, and larger obstacles.

T2 - Demonstrate deployment of a walking robot: A unique deployment process for a walking robot can be achieved, focusing on reducing both the time and risks associated with deployment compared to traditional wheeled rovers. The hypothesis is that a walking rover can be deployed more efficiently with reduced technical complexity and fewer specific components on the lander, leading to a faster and more reliable deployment process. The focus will be on the time required for the deployment, the technical complexity involved, and the number of parts used in the process. The deployment strategy may include innovative approaches, such as deploying the robot without a ramp, potentially using jumping or rolling techniques.

T3 - Demonstrate the ability to use limbs for manipulation: The objective is to demonstrate the ability of robotic limbs to perform measurements and interact with the environment, specifically focusing on manipulating the lunar regolith and moving small rocks. Similar objectives have been successfully demonstrated on Earth [22–24]. This approach can be benchmarked by analyzing interaction forces between the limbs and the regolith, monitoring rock movement and displacement, and evaluating force–displacement curves derived from kinematic and dynamic data. This approach aims to achieve high accuracy and precision in force application and displacement during interactions, allowing soil mechanic experiments along the traverse.

T4 - Demonstrate the use of main-body flexibility: The robot's body can serve as a pan–tilt unit, enabling fixed instruments on the body to achieve the range of motion. The hypothesis is that the robot's body can be effectively utilized to adjust the orientation of onboard instruments by leveraging its range of motion provided by the leg kinematics. Measurements will include the extent of the body's motion and the precision of this motion as monitored through sensors such as an Inertial Measurement Unit (IMU) or kinematic data. This approach aims to simplify the design by eliminating the need for additional pan–tilt mechanisms while still providing the necessary range of motion for the instruments.

T5 - Demonstrate autonomy on the lunar surface: The objective is to advance and demonstrate robot autonomy on the lunar surface, focusing on the ability to adapt and change the level of autonomy based on mission requirements. The hypothesis is that the robot can autonomously traverse a predetermined distance and localize and navigate on the lunar surface with sufficient accuracy and limited human intervention. Additionally, the robot should be capable of mapping the lunar terrain, recognizing environmental characteristics and risks, and suggesting independent decisions to perform specific tasks. Here, we can evaluate the robot's autonomous traversal distance, localization accuracy, navigation efficiency, and decision-making capabilities in various lunar conditions. The goal is to achieve robust autonomy that ensures mission success in dynamic and unpredictable lunar environments.

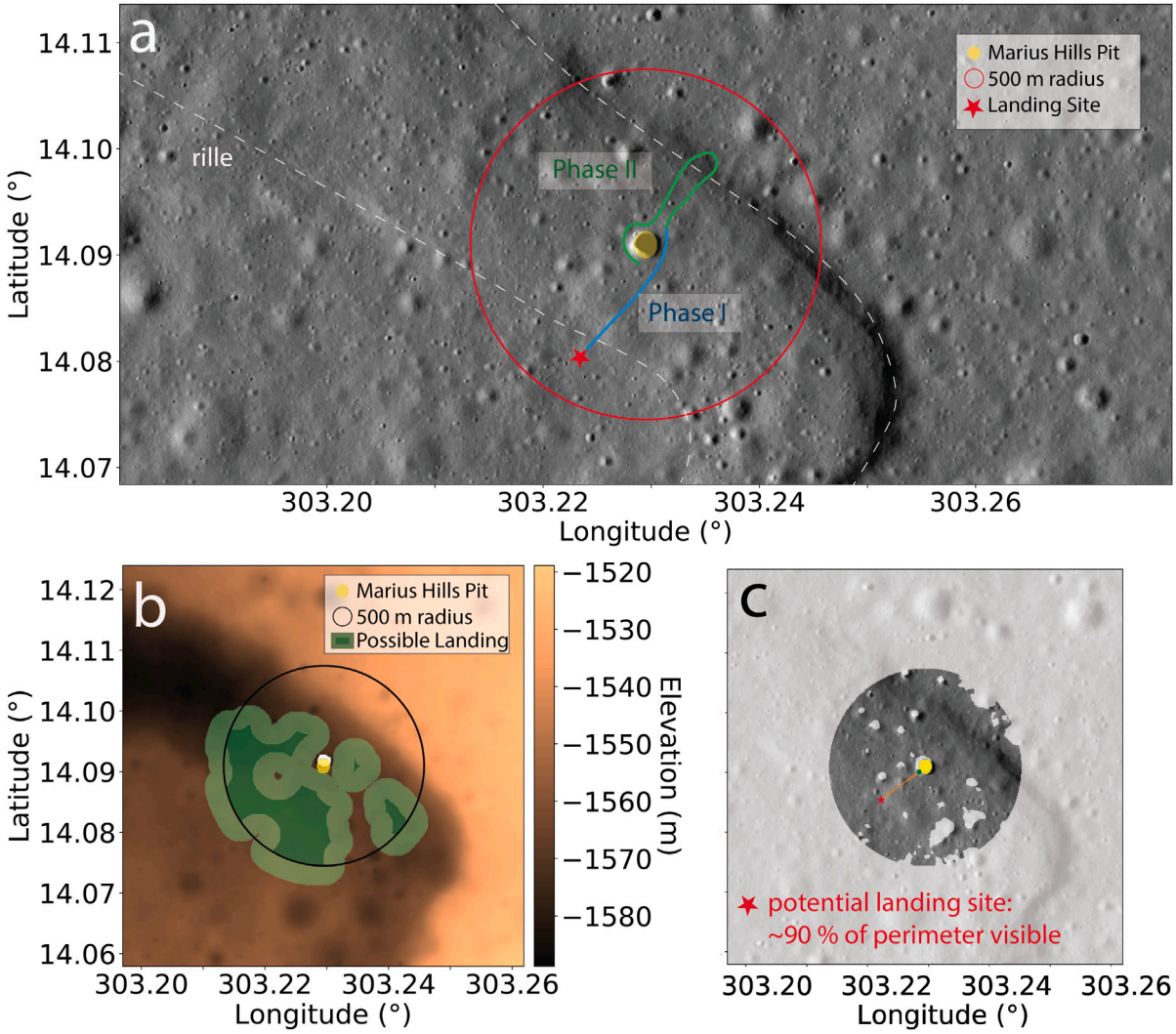

Fig. 3. (a) Foreseen mission traverse from the lander (star) to the MHP in Phase I with an extended traverse as part of Phase II. (b) Possible landing sites are assessed based on slope with a maximum possible slope of 8°. Light green indicates a buffer region associated with landing uncertainty. (c) Visible area from the landing location with the maximum visibility (90.28%), resulting in a minimum walking distance of 250 m (orange line) between the landing location and the pit. Visibility/communication analysis assumes a lander with a 4-m high antenna. (For interpretation of the references to color in this figure legend, the reader is referred to the web version of this article.)

3. Mission concept

3.1. Target site and exploration strategy

LunarLeaper is planned to land on the lunar surface and traverse the lateral extent of the hypothesized subsurface lava tube (Fig. 3) . On its traverse it will take measurements with a ground-penetrating radar (GPR), a gravimeter, and camera images. These measurements will allow us to survey the subsurface structure and detect and map the lava tube geometry if present. After arrival at the pit, the robot will approach the funnel and acquire high-resolution images of the pit walls containing uniquely exposed layers of the geophysically mapped lava flows and regolith layers. These images will not only provide scientific information on lunar volcanism and regolith formation, but also enable assessment of the pit structure stability and its use as a possible lunar base. The mission is expected to last for one lunar day (14 Earth days).

3.2. ConOps

3.2.1. Traverse

We have investigated landing site suitability and a mission traverse around the MHP, with focus on terrain traversability and line-of-sight from a lander. We propose a two-phase approach after landing (Fig. 3a):

Landing: In line with a landing precision of 50 m currently communicated by CLPS landing providers, we require locations within a 100 m circle with <8 degree slope to be considered as possible landing sites (Fig. 3b). For such sites, we test for line-of-sight between landing site and perimeter around the pit.

Phase I: From the landing site, we approach the pit while taking geophysical measurements. When considering a landing site that can provide maximum line-of-sight visibility with any point within a 500 m radius around the pit, the best-case direct walking distance to the pit is ~250 m excluding the traverse around the funnel (Fig. 3c). It consists of a certain periodicity of walking, measurement, data transfer, and

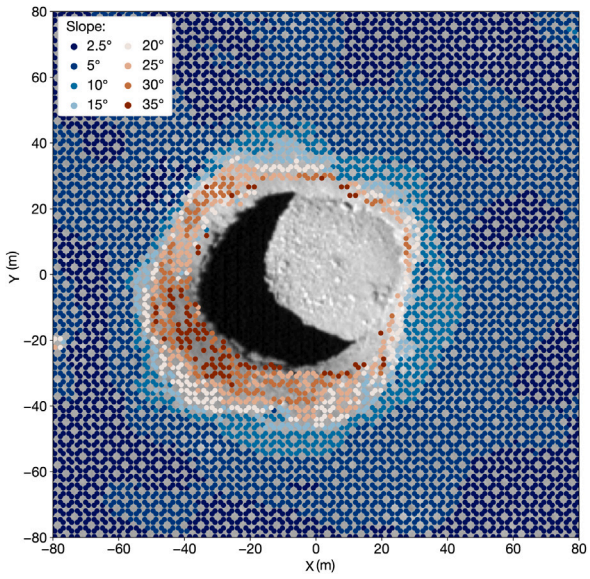

Fig. 4. Slope map around the Marius Hills Pit.

heat management due to the relatively easy terrain, which allows for a certain level of autonomy in the operations. Once arrived at the pit, a careful walk around the pit allows detailed investigation of the opposing wall. As the terrain is significantly more challenging here with slopes reaching up to 35 degrees (Fig. 4), the level of autonomy will be reduced. In total we estimate around 500 m in traveling distance including margin.

Phase II: We continue walking while taking geophysical measurements and crossing the lava tube edge, followed by the return to the pit and in-depth investigation of the opposite pit wall (distance depending on the extent of the traverse, but estimated around 1000 m). Phase I of the traverse will be conducted in the most direct manner to ensure that all primary mission objectives (O1–O4, T1–T4) can be addressed early in the mission, Phase II will include additional elements, such as further technology demonstrations and additional possible scientific investigation of local features such as rocks and regolith.

Our baseline mission does not include the descent into the pit. However, towards the end of the mission and in line with our risk reduction approach, we will investigate the possibility of approaching the pit funnel for a better view of the lower pit sections and possibly the pit floor.

3.2.2. Operational sequence

Derived from the payload requirements regarding measurement intervals, and considering the planned traverse, a refined low-level operational sequence for the ConOps has been developed. This sequence includes platform displacement, measurements, data transmission, navigation re-evaluation, and stand-by phases, each representing distinct operational modes. Measurement durations, power consumption, and data output are determined by the payload specifications, while high-level system assumptions further constrain the remaining parameters.

Fig. 5 illustrates a potential sequence for a nominal case, repeated throughout the mission. It incorporates standby periods, primarily allocated for cooling or recharging, which vary in length with time of day and operational conditions. Measurement intervals are adaptively adjusted within a predefined range during the mission.

This timeline approach facilitates a rough estimate of total power consumption and data generation during the mission. It enables the assignment of mission time to different subsystems.

Mode	Power [W] per Mode	Data [kbyte] per Mode	Time per Mode	Time →				
Baseline	10	0.1	-					
Locomotion/GPR	40	10	4 min					
Gravimeter	10	20	10 min					
Camera/Spectrom	10	1000	1 min					
Communication	20	940	0.5 min					
Stand by	0	0.1	n/a					
		Total Power [W]:		50	20	20	30	10

Fig. 5. Operational sequence of the robot and payloads.

3.2.3. Lunar environment

Gravity is only one-sixth of that on Earth, and the lack of a global magnetic field or substantial atmosphere enhances radiation exposure on the surface [25] and leads to large temperature fluctuations. Furthermore, the surface is constantly affected by impactors of various sizes [26,27]. Our robot will face a challenging environment during the mission, and we will describe three of these challenges related to thermal, and radiation exposure in more detail.

At a latitude of 14 °N, the inclination of the sun is nearly perpendicular [28]. Combined with the lack of atmosphere [29], this results in a significant influx of solar irradiance to the lunar surface, which is mainly modulated by the distance between the Sun and the Moon [30]. In addition to direct solar illumination, a fraction of the incident sunlight is scattered by the lunar regolith [31], that results in diffuse reflection and irradiates the system from below. Consequently, the system's radiator must be oriented and designed to maximize thermal emission to space while minimizing exposure to the Sun and the reflective lunar surface.

Another significant environmental factor comes from the lunar regolith [32,33] and particularly its finest fraction: dust particles with a mean diameter of 60 μm [34]. The dust particles are sharp-edged, like glass [33] and, due to the low electrical conductivity, UV light can build up an electrostatic charge within the particles. The adhesive nature of the dust tends to accumulate on painted surfaces [35]. This dust affects the efficiency of solar panels and radiator surfaces and can also affect joint movements, leading to increased wear [36].

The Moon's radiation environment consists of solar wind, solar energetic particles (SEP), and cosmic galactic rays (CGR). The absence of a magnetosphere and atmosphere allows a high flux of radiation to reach the surface, with pronounced fluctuations correlated to the solar cycle [37,38]. Although the total ionizing dose (TID) accumulated during a 14-day mission is relatively low, the risk of highly energetic particles striking the robot remains significant, potentially causing catastrophic single-event effects. Predicting the probability of such high-energy events, particularly from GCRs, remains challenging. Moreover, as shielding against these impacts is unattainable for small missions, the system design must accommodate this elevated risk or trade its effect on success probability with extra cost.

4. Payload suite

The robot will be equipped with geophysical instruments to enable characterization of the subsurface (Section 4.1,4.2). Further investigation will be dedicated to in-depth visual and possibly spectral characterization of the MHP since the unique capabilities of the robot will allow us to approach the pit despite the steep funnel. Images along the traverse will help interpret the regional geology, including craters or large blocks along the traverse (Section 4.3,4.4). Further, we note that robotic legs enable surface manipulation and probing of geomechanical properties and can be considered part of the mission payload, contributing to both mobility and functional versatility.

4.1. Ground-penetrating radar (GPR)

A GPR is particularly well-suited for detecting subsurface layering and structures. It operates by emitting electromagnetic pulses from an antenna, which are reflected from material interfaces with varying dielectric properties. These variations typically result from differences in porosity or composition, such as between regolith and basaltic bedrock, or between solid rock and void spaces. GPR surveys have been conducted successfully on both the Moon and Mars, providing data on subsurface structures in their dry and cold environments [39,40]. On the Moon, GPR data has been instrumental in constraining regolith thickness, layering across the traversed terrain and inferences regarding the content of TiO_2 and FeO in lunar subsurface material [41–43]. In this mission, the LunarLeaper robot will conduct continuous GPR measurements at intervals of approximately 0.1 m. As it approaches and crosses the presumed boundary of the lava tube, a reflection from the tube ceiling is expected to appear distinctly due to the transition from compact rock to void space, while shallow reflections will represent the boundaries of individual subsurface layers, including the regolith. The GPR antenna detects reflections that are usually represented in radargrams, 2D images showing reflected signal amplitude versus time. Converting GPR travel time to depth relies on a model of the dielectric properties of the lunar regolith and underlying layers, which influence the electromagnetic wave velocity. This model will initially be proposed based on using laboratory measurements from Apollo samples and modeling based on regolith composition and density. Using the hyperbolic shape of reflectors in the radargrams, we can update and refine this prior velocity model [44]. This requires good electromagnetic coupling of the antenna output into the subsurface, specifically an antenna altitude of less than a quarter wavelength, which is enabled the flexibility of a legged system. This finally allows to determine the depth of the reflection patterns corresponding to layers or a void space that would represent the lava tube. The expected data volume is less than 10 kilobytes per observation. For approximately 1 km of traverse, this results in a total data volume of less than 1 gigabyte.

4.2. Gravimeter (GRAV)

Gravimetric methods have long been used to map subsurface structures by detecting density variations [45]. The density contrast between regolith and bedrock makes gravity surveys a valuable tool for identifying structural boundaries. Orbital gravity observations, notably from the GRAIL mission, have revealed key aspects of the lunar crust and interior on scales of kilometers and more [46–50]. Surface gravimeters provide higher resolution and have previously been used successfully. For example, the Traverse Gravimeter Experiment (TGE) was deployed during the Apollo 17 mission and helped identify and characterize a high-density lava flow on the Moon [51,52]. Furthermore, the use of gravimeters mounted on wheeled robotic platforms has previously been proposed for detecting subsurface lava tubes near skylights [53,54].

Here, LunarLeaper will acquire gravity vector measurements at approximately one-meter intervals, providing direct information on the average subsurface density below the robot. After correcting the data for effects not due to subsurface structure (e.g. the altitude and surrounding terrain) [55], gravity data can be inverted for density structure. Here, any additional information such as layering can be used as a prior constraint. The lave tube represents a void space within solid rock, that is, a large density contrast, and the gravimetric signature should provide clear signals, particularly at the transition from rock to lava tube. Additionally, it will allow constraining the density of the ambient rock, which will complement GPR measurements and alleviate ambiguities in interpreting subsurface dielectric properties (e.g., [40]). Since gravimetric methods have poor depth resolution alone, the integration of GPR with gravimetric data has significant benefits. The expected data volume is approximately 20 kilobytes per observation, resulting in less than 20 megabytes for a 1-kilometer survey.

The joint inversion of gravity measurements and GPR combines the methods' individual strengths and will enhance the ability to confirm the presence of a subsurface lava tube and provide robust constraints on its geometry. These combined observations will also facilitate the regional extrapolation of subsurface layers observed along the pit wall and describe the stratigraphy encountered during the traverse.

4.3. Scientific camera (SCAM)

Images play a dual role by providing crucial information for both navigation and site characterization. While satellite imagery has been helpful in identifying potential skylights, high-resolution imaging from the ground offers new detail, particularly for steep and partially overhanging walls, which may be obscured in satellite views. By mounting a high-resolution camera on the tiltable main body of the robot, it is possible to capture images from various angles and locations around the pit. We aim for achieving resolutions of a few centimeters across the pit for illuminated walls and investigate the tradeoff of LED headlights to illuminate deeper regions. These image-based layer and fracture maps will help assess the stability of the pit, enabling advanced modeling to test hypotheses on skylight formation, and evaluate the current and future stability of the lava tubes. We expect to be able to directly map fractures in the photogrammetry model [56] and further use these models to investigate impact processes [57] and thermo-mechanical fatigue. LunarLeaper will acquire images along the traverse providing information on the rock distribution possibly giving clues on the formation process of the pit. At the pit itself, with dense coverage we will create stereo images and generate 3D reconstructions of the pit interior and its funnel at a depth resolution of potentially less than 0.1 m. Depending on the actual depth of the lava tube, it is possible that it can be captured with the camera. The expected data volume of a science camera with a Field of View (FoV) of 40 degrees at 2048x2048 pixel resolution is approximately 2 MB per observation for pit coverage (~30 images) and around 45 high-quality scientific images along the traverse. The total data volume is estimated at 150 MB. Further images will be acquired if bandwidth limitations allow it.

4.4. Spectral assessment (SPEC)

An improved model of the surface-exposed material composition can be provided by assessing their spectral reflectance characteristics. As demonstrated with orbital data using the Lunar Reconnaissance Orbiter Diviner instrument [58], the presence and concentration of rock-forming minerals can be identified by diagnostic spectral features in the thermal infrared wavelength range. The Christiansen feature located between 7.5 and 9 μm is indicative of the total degree of SiO_2 polymerization and together with the reststrahlen/transparency bands (10 to 13 μm) as well as sulfate and phosphate features (8 to 10 μm) minerals like olivine, pyroxene, feldspar, apatite, and ilmenite can be identified [59]. During the next mission design phases, we will investigate the option of adding a MEMS-based Fabry–Perot point spectrometer [60] to better constrain the composition along the pit walls and possibly distinguish source depths of the deposited lava layers. This trade study will take compositional results from landed missions in the CLPS program into account. Expected data volume is <1 Mbyte.

4.5. Payload integration

One key decision is whether to adopt a decentralized architecture, where each payload operates with its own dedicated processor communicating with the main OBC via well-defined protocols, or a centralized system that integrates all payloads into a unified hardware and software platform. While the centralized approach minimizes physical footprint, it also introduces greater system complexity due to the need for extensive cross-talk management.

When fully deployed, the GPR antenna has a total tip-to-tip span of 1.0 m. Its placement is coordinated with the locomotion system to minimize movement constraints while maximizing ground penetration efficiency and overcoming bending cycles over obstacles. During lunar transfer and before deployment, the antenna is stored compactly. The extraction mechanism will pose a challenge for the system design.

5. LunarLeaper robot

The most important technological innovation of this mission is the integrated use of robotic legs. This approach underscores several mission objectives, from the demonstration of autonomous walking and flexibility of the main body to the use of limbs for soil manipulation and deployment. By employing the legs, the robot can access steep areas around the pit, point the thermal radiator directly toward free space and optimize sensor positioning. In the future, this concept may facilitate exploration of the interior of the pit and serve as a modular platform for further missions to the Moon and beyond.

5.1. Related work

Small robotic lunar exploration is thriving, driven by affordable launch opportunities and a growing market for lunar landing providers. Recent missions such as Pragyan [61], Yutu-2 [20], SLIM [62], and the current iSpace Rover [63] underline this trend. Additionally, scheduled projects like the Mobile Autonomous Prospecting Platform (MAPP) rover [64] and CADRE [65], as well as promising approaches like Rashid-1 [66] and the Astrobotics Rover [67], further demonstrate the rapid growth in the field.

Recently, the Pragyan mission successfully landed near the South Pole (69.4 °S), carrying two payloads with a total system weight of 26 kg and a power production of 50 W, operating for one lunar day. Similarly, the CADRE (NASA/JPL) mission is set to land at a comparable latitude (7 °N), in conjunction with the MAPP (Lunar Outpost). The CADRE mission will deploy three autonomous agents equipped with GPR to collaboratively explore the lunar surface, and is designed to operate for one lunar day.

We have actively been conducting research to advance legged robots for planetary exploration [68,69]. Unstructured, natural terrains, characterized by dry granular media, rocks, and slopes, present an ideal challenge for these systems [14,15]. In particular, the development of SpaceBok [12] and SpaceHopper [70] (Fig. 9) has been tailored for such environments. Further analysis, in the context of a potential legged mission to the Moon, confirmed the thermal feasibility of the concept through a first-order approximation [71].

Key learnings from the review of other space robot concepts are multifaceted and offer valuable insights for our design. First, placing motors on the exterior has proven effective for regolith interaction, though it requires robust sealing to protect against abrasive dust. Several missions have also successfully integrated electronics from the private market, demonstrating the viability of leveraging commercial off-the-shelf components. An operational strategy commonly observed is the transition between active and hibernation modes, which optimizes energy consumption and thermal management. In addition, the use of batteries capable of operating in wide temperature ranges enhances the resilience of the system. Finally, a notable design feature is the incorporation of a large, flat radiator on top, with heat-emitting components directly bolted underneath, effectively managing the thermal load.

5.2. Approach and methodology

In the scope of this work we developed a high-level robot design that integrates a suite of COTS components with several key assumptions (see Fig. 7) with each mode linked to a dedicated configuration aimed at optimizing overall performance. In this methodology, we define the environmental assumptions and system-level parameters that underpin our design.

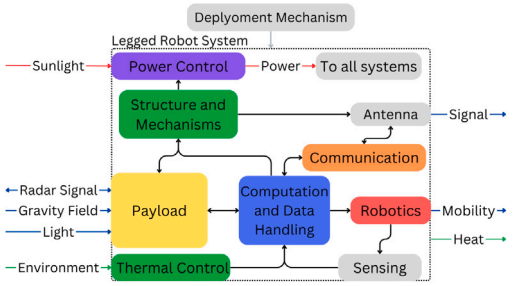

Fig. 6. High-Level Hardware Systems Architecture.

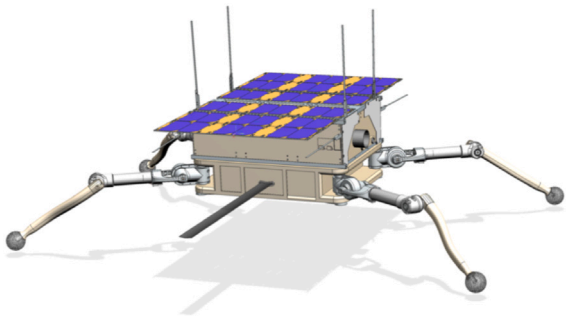

Fig. 7. Early conceptual sketch of the LunarLeaper robot.

5.3. System overview

The system architecture (Fig. 6) is based on the guidelines established by small spacecraft design manuals [72], with the addition of a robotics system that provides attitude control and locomotion for the robot. At the core of the system is the computation and data handling (CDH) unit, which directly connects to the communication system for data transmission and command. The computation system is assumed to be divided into two parts: a low-power onboard computer (OBC) for basic operations and a high-power, high-computation unit for more intensive processing tasks. The robotics system is integrated into a feedback loop with the sensing system, which provides data from both exteroceptive and proprioceptive sensors. The sensing system is also used to localize the robot in the world frame and estimate its current state.

The structure and mechanism system provides the framework for the robot, including interfaces for mechanisms such as deployment systems, antenna extension, and solar panels. The thermal control system regulates the internal temperature, maintaining the internal temperature within operational limits, preferably through passive means. All payloads are directly connected to the CDH system. The robot integrates commercially available off-the-shelf (COTS) components wherever possible, in order to advance the overall technology readiness level (TRL) of the system.

5.4. Mobility and locomotion

The robotics subsystem is central to the mission, serving not only as the primary means of locomotion, but also as an enabler for advanced operational modes. The selection of either mammal-type or spider-type leg configuration, each offering unique benefits in terms of range of motion, terrain interaction, and attitude control, remains under evaluation. The choice between dynamic and static gaits will be determined by specific mission requirements, such as the frequency of crouching maneuvers during the traverse, and the overarching risk policy. Initial locomotion studies have provided estimates for power consumption and velocity, laying the groundwork for further refinement.

5.5. Power and thermal control system

The mission duration is set at 14 Earth days, with power consumption expected to range between 10 W to 50 W. Given these parameters, the most promising power solution is a combination of solar power and battery storage. The power system consists of two deployable solar panels, mounted on both sides of the robot, and a Power Conditioning and Distribution Unit (PCDU), which connects the solar panels and a battery. The PCDU regulates the set points of the solar panels, controls the charge and discharge of the battery, maintains the activity of the Battery Management System (BMS), and provides power at different voltage levels [72]. These units are well-established in spacecraft technology and are compatible with the PC-104 standard [73].

During the preliminary analysis, a battery capacity of 100 Wh provides sufficient margins for all phases. The primary driver of battery size is activity during the first and last 24 h of the mission. Batteries traditionally impose strict limits on the operating temperature of spacecrafts, but advances in research have enabled a wider operational temperature window (−40 °C to 85 °C) [74]. With two solar panels, each measuring 0.3 m by 0.2 m (6U configuration), we expect a peak power output of 40 Wp at the start of the mission. Degradation of the solar panels during the mission has two main contributors: lunar dust and radiation damage (see Section 3.2.3). Dust primarily originates from electrically charged particles accelerated near the terminator, as well as human-induced landing plumes. For short-duration lunar missions, dust accretion of regolith outweighs the effects of long-term radiation damage. Chang'e-3 recorded a deposition of $0.83\,\mathrm{mg\,cm^{-2}}$ on a horizontal collector during its first lunar day at a young mare site, a load sufficient to decrease the output current by 16% [75]. Laboratory tests on partially obscured solar panels show a convex relationship between output power and obscured area, with a current drop of around 35% for a deposition of $2.23\,\mathrm{mg\,cm^{-2}}$ of regolith [76].

Data from the Apollo missions analyze long-term effects and attribute degradation to cosmic particle radiation and ultraviolet light. The performance drop due to radiation damage is estimated at around 0.8% per six months [77,78]. Overall, data on lunar dust and its effect on solar power generation are limited to specific cases and remain scarce, making reliable degradation estimates difficult. Additionally, the legs of our robot introduce a new challenge by adding unknown dynamics of dust kick-up during locomotion. This requires a dedicated study on the behavior and impact of lunar regolith, including the development of a model and simulation throughout the mission.

For solar panels, systems from Endurosat[1] and Gom Space were investigated, as well as satellite drives from Revolv.[2] Feasible PCDU solutions were identified from ISIS[3] and GAUSS,[4] while batteries from Saft[5] or Murata[6] meet the mission requirements.

The thermal design focuses on passive control mechanisms wherever possible, using fail-safe technologies to ensure reliability. The system consists of an insulated box, equipped with solar panels and a radiator on top, optimizing thermal management. The thermal mass is modeled as the main body frame, to which all heat-emitting components are connected. In practice, additional heat sinks are also incorporated. Thermal straps efficiently direct heat flow from the mass to the radiator, ensuring optimal heat dissipation (see Fig. 8).

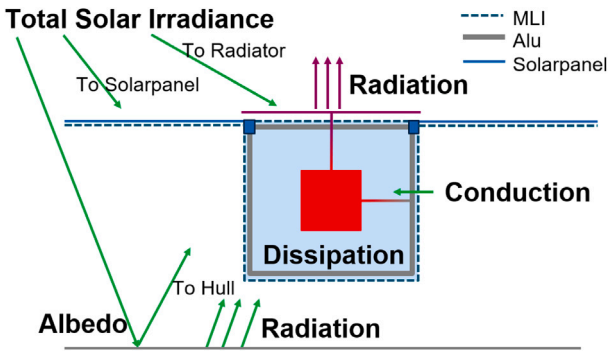

Fig. 8. Thermal heat flow of the robot concept.

For insulation, multi-layer insulation (MLI)[7] is assumed, with a heat transfer coefficient between $0.01\,\mathrm{W\,m^{-2}\,K^{-1}}$ to $0.1\,\mathrm{W\,m^{-2}\,K^{-1}}$, depending on the amount of layers. The exterior hull is coated with specialized materials that meet emissivity and absorptivity requirements for both infrared and solar radiation [79]. These coatings are also designed to resist the adhesion of lunar dust, further enhancing thermal performance. To limit heat transfer through the solar panels, a decoupling material like Glass Fiber Polymer is used, ensuring effective thermal isolation.

The heat flow was modeled using first-principle equations according to [80]. Managing heat is a primary concern for this mission, particularly during the extreme conditions of morning and midday. We identified three key free variables:

Radiator Surface: We assume a top-mounted radiator whose dimensions and material are determined by the system's thermal requirements. Although the baseline design uses a flat radiator, alternative configurations are being evaluated to optimize heat dissipation under peak thermal loads.

Concept of Operations: Optimize system activity during specific periods of the day to maximize performance.

Operating Temperature: Allow for a higher internal temperature to enhance heat dissipation through the radiator.

5.6. Communication

The primary communication link for the robot is the Lander-to-Rover system, while the relay to Earth is assumed to be covered under the launch provider's contract. Furthermore, a service provider is required to transmit data from the Ground Station to a Mission Control Center, with the latency expected to remain under 10 s.

The total data volume for the mission is estimated based on the minimal measurements required from each payload, plus additional data for system health monitoring, resulting in approximately 650 MB. Uplink data is assumed to be negligible, and the downlink data rate is estimated at 250 kbps. From an operational (ConOps) perspective, data transmission is assumed to occur in discrete packages at designated transmission windows. Consequently, the robot must be capable of storing data onboard and selecting specific data packages for downlink during these windows. For safety and reliability, it is crucial to detect communication loss and implement recovery strategies, such as returning to a previously known communication point.

The communication system consists of a COTS available radio module that interfaces directly with the OBC and includes multiple antennas for redundancy. A wide variety of software-defined radios are available on the market, with established options from Caesium,[8] Gomspace,[9]

[1] Endurosat: https://www.endurosat.com/products/6u-solar-panel/.
[2] Revolv Space: https://www.revolvspace.com/products/sara.
[3] ISIS PCDU: https://www.isispace.nl/product/compact-eps/.
[4] GAUSS PCDU: https://www.gaussteam.com/pcdu/.
[5] Saft battery: https://saft4u.saft.com/en/product/mp-small-vl.
[6] Murata battery: https://www.murata.com/products/batteries/cylindrical.

[7] Beyond Gravity MLI: https://www.beyondgravity.com/en/satellites/thermal-control-solutions/satellite-insulation.
[8] CesiumAstro Radio: https://www.cesiumastro.com/.
[9] Gomspace Radio: https://gomspace.com/shop/subsystems/communication-systems/default.aspx.

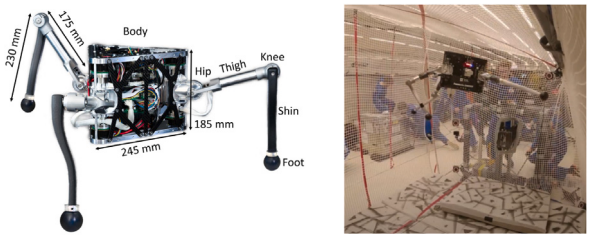

(a) (b)

Fig. 9. The SpaceHopper robot (a) from [70] and (b) during ESA's 83rd Parabolic Flight Campaign.

and Endurosat.[10] A directional antenna will leverage the robotics platform for pointing, with an increased bandwidth when possible, while an omnidirectional antenna will serve as a backup, ensuring continuous connectivity. For the ideal landing site, analysis shows that line-of-sight communications can be maintained for most of the operational time within a 500 m radius (Fig. 3c).

5.7. Autonomy and navigation

We use a scalable autonomy approach [81] with multiple autonomy levels with which the human operator can interact. In our baseline design, we consider three main autonomy levels. At any time, the robot is supervised by a human operator, and the operator can interrupt the robot's operation and interact on multiple levels.

5.7.1. Autonomous operation under human supervision

The highest level of autonomy is mostly aimed at the traverse to the pit. The robot autonomously follows globally defined paths by localizing in the global reference frame and using a local navigation planner to avoid obstacles. The scheduler triggers different robot modes based on pre-defined intervals (for the measurements) or environment parameters (for switching to standby) (see Fig. 5). This mode allows for a fast traverse speed while still ensuring the robot's safety and a high scientific return.

5.7.2. Task-level autonomy

In the intermediate autonomy mode, the user sends task goals. These tasks can include navigation targets that are a few meters away from the robot, measurement requests, or going to other robot modes (i.e. communication, standby). This autonomy level allows for a swift interaction with the robot, while leaving detailed decisions, such as where exactly to move and measure, to the human operator.

5.7.3. Direct teleoperation

The lowest level of autonomy is a backup mode in which the operator sends direct twist commands to the robot. This mode might be needed in case the navigation planner is unavailable, for example if the perception system fails. However, direct teleoperation over the delayed network leads to very slow operation and thus reduced scientific return.

[10] Endurosat Radio: https://www.endurosat.com/products/uhf-transceiver-ii/.

5.8. Feasibility study results

We assessed the overall viability of the mission by integrating the thermal model with other critical robot parameters, including power generation, communication system, and locomotion dynamics, while also accounting for environmental factors. These high-level assumptions allow us to predict overall system performance throughout the mission. The boundary conditions for the assessment are set as follows: to account for indirect paths and to add a buffer for landing uncertainty, we set the baseline walking distance for accomplishing Phase I of the mission at 500 m with measurements performed at defined intervals. Along the path, the state of charge must remain within the limits specified by the power control system. The internal temperature must stay within the assumed bounds for the worst-case hot and cold scenarios. The resulting performance metrics offer a high-level evaluation of the selected system throughout the duration of the mission. While these results guide the design direction, more detailed, time-dependent modeling of temperature and power dynamics is required moving forward.

Thermal: The systems internal temperature is influenced by two dynamic components, the slow but intense external heat fluctuations driven by solar radiation, and rapid changes resulting from the heat dissipation of electronics during active periods. These findings indicate that mission activities must be scheduled taking into account solar illumination. For example, complete hibernation phases may be necessary during noon to prevent overheating.

Power: Solar input varies with solar position, and the efficiency of the solar panels at end-of-life will be critical, as dust buildup diminishes their performance. With the selected components, power management becomes particularly challenging during the transition to lunar night. This analysis underscores the need to limit operations during these periods. Note that extended lunar night operations would require significantly greater energy storage and the mission is currently planned to not last beyond the lunar day.

In its current state, numerous approximations have been made to rapidly assess the feasibility of the mission. For instance, the thermal model is derived from first-principle calculations and does not account for the robot's precise positioning relative to the Sun. Additionally, the power consumption of the legs is represented by a fixed value, as a detailed conceptual analysis is still pending. The integration and placement of all COTS components has been preliminarily deemed feasible from both thermal and electrical perspectives, but further validation is required. Moving forward, the simulation fidelity will be iteratively enhanced to more accurately reflect real-world conditions.

6. Mission implementation

6.1. Programmatics

We currently estimate the total mission cost, including launch, to be 40 million Euros, excluding a 25% contingency, bringing the available mission budget to 50 million Euros. The budget allocation has been carefully structured across different mission stages (pre-Phase A to launch) over a planned five-year duration.

Pre-Phase A: For the system and the core technology identified, we outlined a technology development plan. Critical subsystems that require significant maturation of the TRL have been prioritized for engineering model development.

Phase A: Engineering models (EM) will be developed for critical subsystems (Robot leg mechanism, Energy & Thermal control system, Locomotion control and Autonomy, etc.). We will use our facilities and external facilities to demonstrate system performance in simulated lunar environments. Initial testing will demonstrate feasibility, allow TRL advancement and harmonization of all components to >TRL 6, and inform design of the flight system.

Phase B: A complete engineering model (EM) of the robot will be integrated and tested in relevant, simulated lunar environments. We will develop and test the high level navigation and autonomy strategies as a focus, as well as demonstrate dust/regolith ingress protection. Terrestrial analog testing of science payload will be conducted.

Phase C: Flight design will be finalized, and fabrication will begin following a successful Critical Design Review (CDR). Ground support systems and test procedures will be developed in preparation for flight integration and testing.

Phase D: We will produce the Flight/Qualification unit and test it for launch. We will determine the sparing/qualification unit philosophy in Phase B/C.

The cost items besides the mission planning & management include the engineering design, consisting of modeling of critical subsystem functionality (thermal, power, operation, etc.), design and prototyping mechanical and electrical parts of the system, as well as building up the ground system. For hardware costs, we intend to source components with high TRL and build a flight and an engineering model. For payloads, we rely on existing systems with a high TRL. The software development is another key element, which requires writing of space-ready software according to standard. Testing and validation will be largely performed by team members, who have access to analog missions and have dedicated testing facilities. Further validation capabilities for (subsystem) environmental systems will be available on a contractual basis with industry. We foresee carrying out standard thermal, radiation, vacuum, shock & vibration, dust and electromagnetic compatibility (EMC) testing. The Integration & Assembly is planned to be performed partially in-house and partially at external facilities.

Lastly, to deliver the robot to the lunar surface, we rely on a partnership with commercial or national launch providers. The standard rate among companies currently offering such services is 1 million USD/kg. We anticipate this cost will remain stable or decrease as the number of successful landings grows and market competition becomes more established.

6.2. Risk assessment and mitigation

We performed a detailed risk assessment and mitigation strategy according to the guidelines of the ESA-ECSS-M-00-03 A Risk Management procedure. The risks are structured in scientific, technical, programmatic, operational, environmental, and external challenges.

6.2.1. Scientific risks

We identified three main scientific risks. First, rover- and surface-induced artifacts could impact GPR data interpretation; to mitigate this, the antenna and robot are designed together to minimize artifacts, drawing on experience from the Perseverance mission, and validated through field testing. Second, potential instrument underperformance is addressed through robust modeling of lunar subsurface conditions and design redundancies: the GPR and gravimeter can independently confirm key hypotheses, and navigation cameras can supplement data if needed. Lastly, the risk of a shortened mission is mitigated by structuring the traverse in two phases, ensuring critical scientific objectives are prioritized early, even if the mission duration is reduced.

6.2.2. Technical risks

We identified seven technical risks. Power system failures are mitigated by designing the locomotion system to remain safe during instantaneous power loss. If a higher power consumption is detected than expected, we can adjust locomotion strategies to include more charging stops at the cost of more detailed scientific data. Currently, thermal management risks arise from passive thermal coupling of elements of the robot which can be compromised as a result of the launch. Thorough vibration testing of all components will be required to ensure integrity after launch. To manage communication delays and blackouts, the robot will feature self-diagnosis and recovery functions, with pre-mapped line-of-sight communication plans. In case of actuator failure within the robots legs, the robot will be trained with alternative locomotion gaits to continue operations at reduced speed. Protecting the main computer from damage due to shock or the environment is essential and the risk of breaking is foreseen to be mitigated by packaging electronics with dampening and verifying robustness through drop tests. Payload interference risks will be minimized via extensive integration testing, while structural integrity issues will be addressed through FEM analysis and vibration testing for different load cases.

6.2.3. Programmatic risks

We identified four programmatic risks. The deployment of the robot to the surface remains an open challenge, it is mitigated by designing flexible deployment strategies, including options for the robot to "hop" or "walk off" the lander, with final selection based on the chosen landing provider. To manage the low initial TRL of the legged robot, the usage of conventional technologies with flight heritage is prioritized, modular development is emphasized, and engineering and scientific leadership are co-located to streamline progress. The risks of slow design maturity are addressed through frequent interdisciplinary interaction, a compact team structure for rapid iteration, and the use of external domain expertise when necessary. The risk of not achieving an ideal lunar landing site is mitigated by performing a comprehensive global analysis of the pits and maintaining continuous engagement with multiple landing providers and potential partner missions to maximize flexibility.

6.2.4. Operational risks

We identified five operational risks. Communication delays between the lunar surface and Earth may be introduced due to the lander communication windows and other factors. This risk is mitigated by designing the robot with a high degree of autonomous operational capability, thus reducing the reliance on continuous operator intervention. Risks associated with navigational errors, due to potential sensor degradation or human error, have been acknowledged and will be further mitigated through redundancy concepts and operator training. Inadequate qualification and testing, particularly in replicating lunar conditions such as reduced gravity, are addressed through a combination of extensive physical testing, supplemented by high-fidelity simulations, and the application of conservative design safety margins. To mitigate risks related to faulty autonomy logic or perception errors, the system will undergo statistical modeling in simulation and through selected analog field campaigns. Furthermore, potential challenges arising within the Concept of Operations, such as reduced locomotion speed or suboptimal landing locations, are mitigated through conservative mission planning, including the use of a traverse velocity of 0.2 m/s and a phased mission approach that prioritizes early achievement of critical scientific objectives.

6.2.5. Environmental risks

We identified nine environmental hazards associated with lunar surface operations. To manage the extreme thermal fluctuations and vacuum conditions, extensive subsystem testing in lunar-like environments, including (dirty) thermal vacuum chambers, is planned, supported by thermal modeling and simulation. Risks posed by lunar regolith, such as abrasion, mechanical interference and sinkage, are mitigated by developing dust-tolerant systems, for example with the use of protective sleeves, and optimizing robotic foot designs to reduce sinkage. Radiation and single-event upsets (SEUs) are addressed through the integration of radiation shielding, with the relatively short mission duration reducing cumulative exposure concerns. Risks from micrometeoroid impacts, vacuum degradation of materials, and cumulative component degradation during transport and mission are mitigated through material selection informed by NASA database and

environmental testing. To address risks of temperature peaks beyond expected margins, the robot will autonomously enter a hibernation mode to prevent thermal overload. Mobility hazards due to uneven terrain are mitigated through extensive testing with regolith simulators and the use of a high-degree-of-freedom legged platform capable of self-recovery. Finally, the potential damage to solar panels from terrain-induced incidents is minimized by segmenting the panels, ensuring that partial damage does not critically compromise the energy supply, allowing operational adjustments as necessary.

6.2.6. External risks

We identified five external risks associated with lunar surface operations inherent to lunar exploration via rideshare opportunities. In the event of a lander crash, if the robot remains functional, flexible deployment strategies and the robot's adaptability will be investigated to attempt mission salvage. Launch schedule delays are mitigated by planning for mission timeline adjustments, including compensatory movement strategies to maximize scientific output within shortened windows. Geopolitical risks affecting component procurement and launch opportunities are addressed through diversified component sourcing strategies and proactive engagement with multiple lander providers. To mitigate the risk of third-party payload interference, the team maintains flexible integration strategies and continuous monitoring of mission configurations. Finally, the risk of damage during transport or launch is mitigated through rigorous vibration testing to ensure that the robot can withstand launch and transfer environments.

7. Conclusion

In conclusion, the LunarLeaper mission concept presents a novel approach for exploring lunar pits, potential entry points to subsurface lava tubes on the Moon. By deploying a robot equipped with geophysical instruments such as a GPR and a Gravimeter, the mission is able to investigate the existence of lunar caves and their potential as shelters for future human explorers. Furthermore, detailed imaging and geophysical mapping of the pit and surrounding volcanic features will provide new insights into lunar volcanic history and regolith formation.

Beyond its immediate scientific objectives, the first-time deployment of a legged robot will demonstrate the viability of a novel, disruptive technology for planetary exploration. Validating the technology objectives will pave the way to access hard-to-reach yet scientifically interesting terrain on the Moon, Mars, asteroids, and beyond.

8. Future work

The immediate next steps involve preparation for the System Requirements Review (SRR). This critical phase will require the formal definition and validation of system-level requirements, informed by preliminary feasibility analysis and risk assessments. Key efforts will include refining the mission concept of operations with greater granularity, finalizing payload integration strategies, and maturing subsystem designs, particularly focusing on the locomotion, thermal, and communication system. In addition, emphasis will be placed on detailed modeling of environmental interactions, such as dust mitigation and thermal load management, to ensure robust performance under lunar conditions. Parallel efforts will address the development of autonomous algorithms for navigation and operational resilience. Beyond the SRR, subsequent development phases will aim to iteratively validate subsystem performance through analog field campaigns and environmental testing. Collaborations with lunar lander providers and the lunar science community will be pursued to align deployment strategies and optimize scientific return.

CRediT authorship contribution statement

Hendrik Kolvenbach: Writing – original draft, Conceptualization, Writing – review & editing, Supervision, Funding acquisition. **Anna Mittelholz:** Writing – original draft, Conceptualization, Writing – review & editing, Supervision, Funding acquisition. **Simon C. Stähler:** Writing – review & editing, Funding acquisition, Writing – original draft, Conceptualization. **Philip Arm:** Writing – original draft, Formal analysis, Supervision, Conceptualization. **Valentin T. Bickel:** Writing – original draft, Writing – review & editing, Conceptualization. **Adrian Fuhrer:** Writing – original draft, Data curation, Formal analysis. **Jordi Gomez Jodar:** Formal analysis. **Ramon Margarit:** Investigation. **Joseph Church:** Investigation, Conceptualization Supervision. **Elena Krasnova:** Investigation, Conceptualization Supervision. **Krzysztof Walas:** Conceptualization. **Matthias Grott:** Conceptualization. **Svein-Erik Hamran:** Conceptualization. **Özgür Karatekin:** Conceptualization. **Miguel Olivares-Mendez:** Conceptualization. **Sofia Coloma:** Conceptualization, Writing – review & editing. **Marco Pagnamenta:** Conceptualization. **Michał Gumiela:** Conceptualization. **Jordan Aaron:** Conceptualization, Writing – review & editing. **Marco Hutter:** Supervision, Conceptualization, Funding acquisition.

Declaration of competing interest

The authors declare that they have no known competing financial interests or personal relationships that could have appeared to influence the work reported in this paper.

Acknowledgments

LunarLeaper acknowledges funding through the CHiwi Foundation and SERI's NASO program (1-012571, LunarLeaper 2024). AM acknowledges funding through SNF Ambizione grant number PZ00P2_209123.

References

[1] R.V. Wagner, M.S. Robinson, Lunar pit morphology: Implications for exploration, J. Geophys. Res.: Planets 127 (8) (2022) e2022JE007328.

[2] Francesco Sauro, Riccardo Pozzobon, Matteo Massironi, Pierluigi De Berardinis, Tommaso Santagata, Jo De Waele, Lava tubes on earth, moon and mars: A review on their size and morphology revealed by comparative planetology, Earth-Sci. Rev. (ISSN: 0012-8252) 209 (2020) 103288, http://dx.doi.org/10.1016/j.earscirev.2020.103288, URL https://www.sciencedirect.com/science/article/pii/S0012825220303342.

[3] Pablo F Miaja, Fermin Navarro-Medina, Daniel G Aller, Germán León, Alejandro Camanzo, Carlos Manuel Suarez, Francisco G Alonso, Diego Nodar, Francesco Sauro, Massimo Bandecchi, et al., RoboCrane: A system for providing a power and a communication link between lunar surface and lunar caves for exploring robots, Acta Astronaut. 192 (2022) 30–46.

[4] Donald M Hooper, Samuel W Ximenes, Edward L Patrick, Ronald Wells, Allison Shaffer, Marius Necsoiu, Leto mission concept for green reconnaissance of the Marius Hills Lunar Pit, Planet. Sci. J. 4 (2) (2023) 26.

[5] Junichi Haruyama, Kazuyuki Hioki, Motomaro Shirao, Tomokatsu Morota, Harald Hiesinger, Carolyn H. van der Bogert, Hideaki Miyamoto, Akira Iwasaki, Yasuhiro Yokota, Makiko Ohtake, Tsuneo Matsunaga, Seiichi Hara, Shunsuke Nakanotani, Carle M. Pieters, Possible lunar lava tube skylight observed by SELENE cameras, Geophys. Res. Lett. 36 (21) (2009) http://dx.doi.org/10.1029/2009GL040635, arXiv:https://agupubs.onlinelibrary.wiley.com/doi/pdf/10.1029/2009GL040635.

[6] MS Robinson, JW Ashley, AK Boyd, RV Wagner, EJ Speyerer, B Ray Hawke, H Hiesinger, CH Van Der Bogert, Confirmation of sublunarean voids and thin layering in mare deposits, Planet. Space Sci. 69 (1) (2012) 18–27.

[7] Loic Chappaz, Rohan Sood, Henry J Melosh, Kathleen C Howell, David M Blair, Colleen Milbury, Maria T Zuber, Evidence of large empty lava tubes on the moon using GRAIL gravity, Geophys. Res. Lett. 44 (1) (2017) 105–112.

[8] Leonardo Carrer, Riccardo Pozzobon, Francesco Sauro, Davide Castelletti, Gerald Wesley Patterson, Lorenzo Bruzzone, Radar evidence of an accessible cave conduit on the moon below the mare tranquillitatis pit, Nat. Astron. (ISSN: 2397-3366) (2024) http://dx.doi.org/10.1038/s41550-024-02302-y.

[9] Joonho Lee, Jemin Hwangbo, Lorenz Wellhausen, Vladlen Koltun, Marco Hutter, Learning quadrupedal locomotion over challenging terrain, Sci. Robot. 5 (47) (2020) eabc5986.

[10] David Hoeller, Nikita Rudin, Dhionis Sako, Marco Hutter, Anymal parkour: learning agile navigation for quadrupedal robots, Sci. Robot. 9 (88) (2024) eadi7566, http://dx.doi.org/10.1126/scirobotics.adi7566.

[11] Takahiro Miki, Joonho Lee, Jemin Hwangbo, Lorenz Wellhausen, Vladlen Koltun, Marco Hutter, Learning robust perceptive locomotion for quadrupedal robots in the wild, Sci. Robot. 7 (62) (2022) eabk2822.

[12] Philip Arm, Radek Zenkl, Patrick Barton, Lars Beglinger, Alex Dietsche, Luca Ferrazzini, Elias Hampp, Jan Hinder, Camille Huber, David Schaufelberger, Felix Schmitt, Benjamin Sun, Boris Stolz, Hendrik Kolvenbach, Marco Hutter, Spacebok: a dynamic legged robot for space exploration, in: Proceedings of the 2019 IEEE International Conference on Robotics and Automation (ICRA 2019), IEEE, 2019, pp. 6288–6294, http://dx.doi.org/10.1109/ICRA.2019.8794136.

[13] Marco Hutter, Christian Gehring, Andreas Lauber, Fabian Gunther, Carmine D. Bellicoso, Vassilios Tsounis, Péter Fankhauser, Remo Diethelm, Samuel Bachmann, Michael Bloesch, Hendrik Kolvenbach, Marko Bjelonic, Linus Isler, Konrad Meyer, Anymal — toward legged robots for harsh environments, Adv. Robot. 31 (17) (2017) 918–931, http://dx.doi.org/10.1080/01691864.2017.1378591.

[14] Hendrik Kolvenbach, Philip Arm, Elias Hampp, Alexander Dietsche, Valentin Bickel, Benjamin Sun, Christoph Meyer, Marco Hutter, Traversing steep and granular martian analog slopes with a dynamic quadrupedal robot, Field Robot. 2 (1) (2022) 910–939, http://dx.doi.org/10.55417/fr.2022030.

[15] Giorgio Valsecchi, Cedric Weibel, Hendrik Kolvenbach, Marco Hutter, Towards legged locomotion on steep planetary terrain, in: 2023 IEEE/RSJ International Conference on Intelligent Robots and Systems, IROS, IEEE, 2023, pp. 786–792.

[16] Sarah A. Fagents, M. Elise Rumpf, Ian A. Crawford, Katherine H. Joy, Preservation potential of implanted solar wind volatiles in lunar paleoregolith deposits buried by lava flows, Icarus (ISSN: 0019-1035) 207 (2) (2010) 595–604, http://dx.doi.org/10.1016/j.icarus.2009.11.033, URL https://www.sciencedirect.com/science/article/pii/S0019103509004837.

[17] Charles K Shearer, Paul C Hess, Mark A Wieczorek, Matt E Pritchard, E Mark Parmentier, Lars E Borg, John Longhi, Linda T Elkins-Tanton, Clive R Neal, Irene Antonenko, et al., Thermal and magmatic evolution of the moon, Rev. Miner. Geochem. 60 (1) (2006) 365–518.

[18] Jialong Lai, Yi Xu, Roberto Bugiolacchi, Xu Meng, Long Xiao, Minggang Xie, Bin Liu, Kaichang Di, Xiaoping Zhang, Bin Zhou, Shaoxiang Shen, Luyuan Xu, First look by the yutu-2 rover at the deep subsurface structure at the lunar farside, Nat. Commun. (ISSN: 2041-1723) 11 (1) (2020) 3426, http://dx.doi.org/10.1038/s41467-020-17262-w.

[19] Fang Guang-You, Zhou Bin, Ji Yi-Cai, Zhang Qun-Ying, Shen Shao-Xiang, Li Yu-Xi, Guan Hong-Fei, Tang Chuan-Jun, Gao Yun-Ze, Lu Wei, Ye Sheng-Bo, Han Hai-Dong, Zheng Jin, Wang Shu-Zhi, Lunar penetrating radar onboard the chang'e-3 mission, Res. Astron. Astrophys. 14 (12) (2014) 1607, http://dx.doi.org/10.1088/1674-4527/14/12/009.

[20] L. Ding, R. Zhou, Y. Yuan, H. Yang, J. Li, T. Yu, C. Liu, J. Wang, S. Li, H. Gao, Z. Deng, N. Li, Z. Wang, Z. Gong, G. Liu, J. Xie, S. Wang, Z. Rong, D. Deng, X. Wang, S. Han, W. Wan, L. Richter, L. Huang, S. Gou, Z. Liu, H. Yu, Y. Jia, B. Chen, Z. Dang, K. Zhang, L. Li, X. He, S. Liu, K. Di, A 2-year locomotive exploration and scientific investigation of the lunar farside by the Yutu-2 rover, Sci. Robot. 7 (62) (2022) eabj6660, http://dx.doi.org/10.1126/scirobotics.abj6660, arXiv:https://www.science.org/doi/pdf/10.1126/scirobotics.abj6660.

[21] J.N. Rasera, J.J. Cilliers, J.A. Lamamy, K. Hadler, The beneficiation of lunar regolith for space resource utilisation: A review, Planet. Space Sci. 186 (2020) 104879.

[22] Hendrik Kolvenbach, Christian Bärtschi, Lorenz Wellhausen, Ruben Grandia, Marco Hutter, Haptic inspection of planetary soils with legged robots, IEEE Robot. Autom. Lett. 4 (2) (2019) 1626–1632, http://dx.doi.org/10.1109/LRA.2019.2896732.

[23] Philip Arm, Mayank Mittal, Hendrik Kolvenbach, Marco Hutter, Pedipulate: Enabling manipulation skills using a quadruped robot's leg, in: 2024 IEEE International Conference on Robotics and Automation, ICRA, 2024, pp. 5717–5723, http://dx.doi.org/10.1109/ICRA57147.2024.10611307.

[24] Jakub Bednarek, Michał Bednarek, Lorenz Wellhausen, Marco Hutter, Krzysztof Walas, What am i touching? learning to classify terrain via haptic sensing, in: Proceedings of the 2019 IEEE International Conference on Robotics and Automation (ICRA 2019), IEEE, 2019, pp. 7187–7193, http://dx.doi.org/10.1109/ICRA.2019.8794478.

[25] Guenther Reitz, Thomas Berger, Daniel Matthiae, Radiation exposure in the moon environment, Planet. Space Sci. (ISSN: 0032-0633) 74 (1) (2012) 78–83, http://dx.doi.org/10.1016/j.pss.2012.07.014, Scientific Preparations For Lunar Exploration. URL https://www.sciencedirect.com/science/article/pii/S0032063312002085.

[26] NASA, Lunar impact monitoring program, 2023, Last updated October 24, 2023. https://www.nasa.gov. (Accessed 26 January 2025).

[27] Alexander Jablonski, Kelly Ogden, Technical requirements for lunar structures, J. Aerosp. Eng. - J AEROSP ENG 21 (2008) http://dx.doi.org/10.1061/(ASCE)0893-1321(2008)21:2(72).

[28] Marcin Kaczmarzyk, Marcin Gawronski, Grzegorz Piatkowski, Global database of direct solar radiation at the moon's surface for lunar engineering purposes, E3S Web Conf. 49 (2018) 00053, http://dx.doi.org/10.1051/e3sconf/20184900053.

[29] R.R. Jr. Hodges, J.H. Hoffmann, Francis S. Johnson, The lunar atmosphere, Icarus 21 (1974) 415–426.

[30] P. Foukal, C. Fröhlich, H. Spruit, T.M.L. Wigley, Variations in solar luminosity and their effect on the earth's climate, Nature 443 (2006) 161–166, http://dx.doi.org/10.1038/nature05072.

[31] Huazhong Ren, Jing Nie, Jiaji Dong, Rongyuan Liu, Wenzhe Fa, Ling Hu, Wenjie Fan, Lunar surface temperature and emissivity retrieval from diviner lunar radiometer experiment sensor, Earth Space Sci. 7 (10) (2020) http://dx.doi.org/10.1029/2020EA001436, e2020EA001436.

[32] Shuoran Yu, Wenzhe Fa, Thermal conductivity of surficial lunar regolith estimated from lunar reconnaissance orbiter diviner radiometer data, Planet. Space Sci. (ISSN: 0032-0633) 124 (2016) 48–61, http://dx.doi.org/10.1016/j.pss.2016.02.001, URL https://www.sciencedirect.com/science/article/pii/S0032063316000222.

[33] D.S. Mckay, D.W. Ming, Properties of lunar regolith, in: Lowell A. Douglas (Ed.), Soil Micro-Morphology: A Basic and Applied Science, in: Developments in Soil Science, vol. 19, Elsevier, (ISSN: 0166-2481) 1990, pp. 449–462, http://dx.doi.org/10.1016/S0166-2481(08)70360-X, URL https://www.sciencedirect.com/science/article/pii/S016624810870360X.

[34] E.N. Slyuta, Physical and mechanical properties of the lunar soil (a review), Sol. Syst. Res. (ISSN: 0038-0946) 48 (5) (2014) 329–353, http://dx.doi.org/10.1134/S0038094614050050, Original Russian text published in Astronomicheskii Vestnik, 2014, Vol. 48, No. 5, pp. 358–382..

[35] O.E. Berg, F.F. Richardson, J.W. Rhee, S. Auer, Preliminary results of a cosmic dust experiment on the moon, Geophys. Res. Lett. 1 (7) (1974) 289.

[36] Dorota Budzyn, Eoin Tuohy, Natan Garrivier, Timon Schild, Aidan Cowley, Reuben Cruise, Masato Adachi, Hossein Zare-Behtash, Andrea Cammarano, Lunar dust: Its impact on hardware and mitigation technologies, in: Proceedings of the 46th Aerospace Mechanisms Symposium, Virtual, 2022, pp. 287–xxx, NASA, Virtual Conference.

[37] H.W. Babcock, The Topology of the Sun's Magnetic Field and the 22-Year Cycle., Astrophys. J. 133 (1961) 572, http://dx.doi.org/10.1086/147060.

[38] Peter V. Foukal, Solar Astrophysics, WILEY-VCH Verlag GmbH & Co. KGaA, Weinheim, Germany, ISBN: 9783527403745, 2004, http://dx.doi.org/10.1002/9783527602551.

[39] Svein-Erik Hamran, David A Paige, Abigail Allwood, Hans EF Amundsen, Tor Berger, Sverre Brovoll, Lynn Carter, Titus M Casademont, Leif Damsgård, Henning Dypvik, et al., Ground penetrating radar observations of subsurface structures in the floor of jezero crater, mars, Sci. Adv. 8 (34) (2022) eabp8564.

[40] Elena Pettinelli, Barbara Cosciotti, Sebastian Emanuel Lauro, Elisabetta Mattei, An overview of GPR subsurface exploration of planets and moons, Lead. Edge 41 (10) (2022) 672–680.

[41] W. David Carrier III, Gary R. Olhoeft, Wendell Mendell, Physical properties of the lunar surface, Lunar Sourceb. User's Guid. Moon (1991) 475–594.

[42] Wenzhe Fa, Modeling and simulation for ground penetrating radar study of the subsurface structure of the moon, in: 2012 14th International Conference on Ground Penetrating Radar, GPR, IEEE, 2012, pp. 922–926.

[43] Zehua Dong, Guangyou Fang, Bin Zhou, Di Zhao, Yunze Gao, Yicai Ji, Properties of lunar regolith on the moon's farside unveiled by chang'e-4 lunar penetrating radar, J. Geophys. Res.: Planets 126 (6) (2021) e2020JE006564.

[44] Elizabeth Fisher, George A. McMechan, A. Peter Annan, Steve W. Cosway, Examples of reverse-time migration of single-channel, ground-penetrating radar profiles, Geophysics (ISSN: 0016-8033) 57 (4) (1992) 577–586, http://dx.doi.org/10.1190/1.1443271.

[45] John M. Reynolds, An Introduction to Applied and Environmental Geophysics, John Wiley & Sons, 2011.

[46] Maria T Zuber, David E Smith, Michael M Watkins, Sami W Asmar, Alexander S Konopliv, Frank G Lemoine, H Jay Melosh, Gregory A Neumann, Roger J Phillips, Sean C Solomon, et al., Gravity field of the moon from the gravity recovery and interior laboratory (GRAIL) mission, Science 339 (6120) (2013) 668–671.

[47] Mark A Wieczorek, Gregory A Neumann, Francis Nimmo, Walter S Kiefer, G Jeffrey Taylor, H Jay Melosh, Roger J Phillips, Sean C Solomon, Jeffrey C Andrews-Hanna, Sami W Asmar, et al., The crust of the moon as seen by GRAIL, Science 339 (6120) (2013) 671–675.

[48] Jeffrey C Andrews-Hanna, Sami W Asmar, James W Head III, Walter S Kiefer, Alexander S Konopliv, Frank G Lemoine, Isamu Matsuyama, Erwan Mazarico, Patrick J McGovern, H Jay Melosh, et al., Ancient igneous intrusions and early expansion of the moon revealed by GRAIL gravity gradiometry, Science 339 (6120) (2013) 675–678.

[49] Isamu Matsuyama, Francis Nimmo, James T Keane, Ngai H Chan, G Jeffrey Taylor, Mark A Wieczorek, Walter S Kiefer, James G Williams, GRAIL, LLR, and LOLA constraints on the interior structure of the moon, Geophys. Res. Lett. 43 (16) (2016) 8365–8375.

[50] S Goossens, TJ Sabaka, MA Wieczorek, GA Neumann, E Mazarico, FG Lemoine, JB Nicholas, DE Smith, MT Zuber, High-resolution gravity field models from GRAIL data and implications for models of the density structure of the moon's crust, J. Geophys. Res.: Planets 125 (2) (2020) e2019JE006086.

[51] M. Talwani, H.-G. Kahle, Apollo 17 traverse gravimeter experiment/preliminary results, NASA STI/Recon Tech. Rep. A 77 (1976) 85–91.
[52] Natasha Urbancic, R Ghent, Catherine L Johnson, Sabine Stanley, David Hatch, Kieran A Carroll, WB Garry, M Talwani, Subsurface density structure of taurus-littrow valley using apollo 17 gravity data, J. Geophys. Res.: Planets 122 (6) (2017) 1181–1194.
[53] K.A. Carroll, Rover-based system for scouting and mapping lava tubes from the moon's surface using gravimetric surveying: executive summary, (CSYS-ELC-TN-004) Canadensys Aerospace Corporation for the European Space Agency, Bolton, Ontario, Canada, 2021, ESA Contract No. 4000130711/20/NL/GLC.
[54] Kieran A. Carroll, David Hatch, Rebecca Ghent, Sabine Stanley, Natasha Urbancic, Marie-Claude Williamson, W. Brent Garry, Manik Talwani, Exploring lunar sub-surface voids using surface gravimetry, in: 46th Lunar and Planetary Science Conference, 2015, Accompanying abstract: Carroll K.A. et al. (2015) LPS XLVI, Abstract #1746.
[55] D.A.G. Nowell, Gravity terrain corrections — an overview, J. Appl. Geophys. (ISSN: 0926-9851) 42 (2) (1999) 117–134, http://dx.doi.org/10.1016/S0926-9851(99)00028-2.
[56] K Anders, M Hämmerle, G Miernik, T Drews, A Escalona, C Townsend, B Höfle, 3D geological outcrop characterization: automatic detection of 3D planes (azimuth and dip) using lidar point clouds, ISPRS Ann. Photogramm. Remote. Sens. Spat. Inf. Sci. 3 (2016) 105–112.
[57] X.F. Li, H.B. Li, J. Zhao, 3D polycrystalline discrete element method (3PDEM) for simulation of crack initiation and propagation in granular rock, Comput. Geotech. 90 (2017) 96–112.
[58] Paul G. Lucey, Benjamin Greenhagen, Kerri Donaldson Hanna, Neil Bowles, Abigail Flom, David A. Paige, Christiansen Feature Map From the Lunar Reconnaissance Orbiter Diviner Lunar Radiometer Experiment: Improved Corrections and Derived Mineralogy, J. Geophys. Res. (Planets) 126 (6) (2021) e06777, http://dx.doi.org/10.1029/2020JE006777.
[59] K.A. Shirley, T.D. Glotch, Particle Size Effects on Mid-Infrared Spectra of Lunar Analog Minerals in a Simulated Lunar Environment, J. Geophys. Res. (Planets) 124 (4) (2019) 970–988, http://dx.doi.org/10.1029/2018JE005533.
[60] M. Grott, J. Knollenberg, T. Großmann, J. Wecker, J. Martin, A. Ihring, B. Jung, K. Vasiliou, J. Helbert, MEMS based Fabry-Perot interferometers for in-situ material characterization, in: COSPAR 45th Scientific Assembly, vol. B0.2-0010-24, 2024, p. 33468.
[61] Indian Space Research Organisation (ISRO), Chandrayaan-3 details, 2025, https://www.isro.gov.in/Chandrayaan3_Details.html. (Accessed 3 January 2025).
[62] Japan Aerospace Exploration Agency (JAXA), SLIM media kit, 2023, https://global.jaxa.jp/countdown/slim/SLIM-mediakit-EN_2310.pdf. (Accessed 26 January 2025).
[63] ispace inc., ispace-EUROPE Announces Completion of First European Designed, Manufactured, and Assembled Lunar Micro Rover, 2024, Retrieved from a press conference in Luxembourg. Press release.
[64] Sarah Vines, George Ho, David Blewett, The Lunar Vertex PRISM Payload: Ready for the Moon, in: EGU General Assembly Conference Abstracts, in: EGU General Assembly Conference Abstracts, 2024, p. 21717, http://dx.doi.org/10.5194/egusphere-egu24-21717.
[65] Jean-Pierre de la Croix, Federico Rossi, Roland Brockers, Dustin Aigalin, Keenan Allen, Elizabeth Borson, Ashitha Cailici, Juliet Becker, Robert Hewitt, Ben Hogan, Grace Lim, Benjamin Morrell, Yashvanth Nakka, Viet Nguyen, Pedro Proena, Gregg Rabideau, Joseph Russino, Maria Sabido da Silva, Guy Zohar, Subha Comandur, Multi-agent autonomy for space exploration on the CADRE lunar technology demonstration, IEEE Aerosp. Conf. Proc. (2024) http://dx.doi.org/10.1109/AERO58975.2024.10521425,
[66] Reeza Almashri, Pinalet Garg, Mohammed Wali, Thermal management system design and analysis of rashid rover – emirates lunar mission, in: Proceedings of the 72nd International Astronautical Congress, IAC, Dubai, United Arab Emirates, 2021, Paper ID: IAC-21-C2.7, published by the International Astronautical Federation (IAF).
[67] Andrew P. Tallaksen, Andrew D. Horchler, Curtis Boirum, Daniel Arnett, Heather L. Jones, Eugene Fang, Eric Amoroso, Louis Chomas, Lawrence Papincak, Oleg B. Sapunkov, William L. Whittaker, CubeRovers for Lunar Exploration.
[68] Hendrik Kolvenbach, Quadrupedal Robots for Planetary Exploration (Ph.D. thesis), ETH Zurich, IRIS, 2021.
[69] Philip Arm, Gabriel Waibel, Jan Preisig, Turcan Tuna, Ruyi Zhou, Valentin Bickel, Gabriela Ligeza, Takahiro Miki, Florian Kehl, Hendrik Kolvenbach, et al., Scientific exploration of challenging planetary analog environments with a team of legged robots, Sci. Robot. 8 (80) (2023) eade9548.
[70] Alexander Spiridonov, Fabio Buehler, Moriz Berclaz, Valerio Schelbert, Jorit Geurts, Elena Krasnova, Emma Steinke, Jonas Toma, Joschua Wuethrich, Recep Polat, Wim Zimmermann, Philip Arm, Nikita Rudin, Hendrik Kolvenbach, Marco Hutter, SpaceHopper: A small-scale legged robot for exploring low-gravity celestial bodies, in: 2024 IEEE International Conference on Robotics and Automation, ICRA, 2024, pp. 3464–3470, http://dx.doi.org/10.1109/ICRA57147.2024.10610057.
[71] Marco Trentini, Philip Arm, Giorgio Valsecchi, Hendrik Kolvenbach, Marco Hutter, Concept study of a small-scale dynamic legged robot for lunar exploration, in: IAC 2023 Conference Proceedings, International Astronautical Federation, 2023, p. 78250.
[72] Small Spacecraft Systems Virtual Institute, State-of-the-Art Small Spacecraft Technology, National Aeronautics and Space Administration (NASA), Ames Research Center, Moffett Field, CA 94035-1000, 2024, NASA Technical Publication NASA/TP–Juliet Becker, Robert Hewitt, Ben Hogan, 2024–0001462. Available from NASA Center for AeroSpace Information, Hanover, MD. URL http://www.nasa.gov/smallsat-institute/sst-soa.
[73] PC/104 Embedded Consortium, PC/104 Specification Version 2.6, 2008, Copyright 1992–2008 by PC/104 Embedded Consortium.http://www.pc104.org.
[74] John-Paul Jones, Marshall C. Smart, Frederick C. Krause, William C. West, Erik J. Brandon, Batteries for robotic spacecraft, Joule (ISSN: 2542-4351) 6 (5) (2022) 923–928, http://dx.doi.org/10.1016/j.joule.2022.04.004, URL https://www.sciencedirect.com/science/article/pii/S2542435122001428.
[75] HaiYan Zhang, Yi Wang, LiPing Chen, He Zhang, CunHui Li, JianHong Zhuang, DeTian Li, YongJun Wang, ShengSheng Yang, XiongYao Li, WeiDong Wang, In-situ lunar dust deposition amount induced by lander landing in chang'e-3 mission, Sci. China Technol. Sci. (ISSN: 1869-1900) 63 (3) (2020) 520–527, http://dx.doi.org/10.1007/s11431-019-1434-y.
[76] Javad Shahmoradi, Austin Maxwell, Summer Little, Quincy Bradfield, Sayavur Bakhtiyarov, Pedram Roghanchi, Mostafa Hassanalian, The effects of martian and lunar dust on solar panel efficiency and a proposed solution, in: AIAA Scitech 2020 Forum, American Institute of Aeronautics and Astronautics, Orlando, FL, 2020, http://dx.doi.org/10.2514/6.2020-1550, URL http://arc.aiaa.org.
[77] J.R. Bates, P.H. Fang, Some astronomical effects observed by solar cells from apollo missions on lunar surface, Sol. Energy Mater. Sol. Cells (ISSN: 0927-0248) 68 (1) (2001) 23–29, http://dx.doi.org/10.1016/S0927-0248(00)00343-3.
[78] J.R. Bates, P.H. Fang, Results of solar cell performance on lunar base derived from apollo missions, Sol. Energy Mater. Sol. Cells (ISSN: 0927-0248) 26 (1) (1992) 79–84, Received 16 August 1991.
[79] Edward M. Silverman, Space Environmental Effects on Spacecraft: LEO Materials Selection Guide, Part 2, NASA. TRW, Inc., Redondo Beach, CA, United States, 1995, Legacy CDMS. Contractor Report (CR) NASA-CR-4661-PT-2. Work of the US Government. Public Use Permitted..
[80] Giorgio Valsecchi, Davide Liconti, Fabian Tischhauser, Hendrik Kolvenbach, Marco Hutter, Preliminary design of actuators for walking robot on the moon, ETH Zurich, Institute of Robotics and Intelligent Systems, Zurich, 2022-06, http://dx.doi.org/10.3929/ethz-b-000547047, 16th Symposium on Advanced Space Technologies in Robotics and Automation (ASTRA 2022); Conference Location: Noordwijk, Netherlands; Conference Date: June 1-2, 2022; Conference lecture held on June 1, 2022.
[81] Georg Rudnick, Axel Schulte, Scalable autonomy concept for reconnaissance UAVs on the basis of an HTN agent architecture, in: 2016 International Conference on Unmanned Aircraft Systems, ICUAS, IEEE, 2016, pp. 40–46.